Anomalous breakdown of Bloch's rule in the Mott-Hubbard insulator $MnTe_2$

Tapan Chatterji,[1] Antonio M. dos Santos,[2] Jamie J. Molaison,[2] Thomas C. Hansen,[1] Stefan Klotz,[3] Mathew Tucker,[4] Kartik Samanta,[5] and Tanusri Saha-Dasgupta[5]

[1]*Institut Laue-Langevin, Boîte Postale 156, 38042 Grenoble Cedex 9, France*

[2]*Quantum Condensed Matter Division, Oak Ridge National Laboratory, Oak Ridge, Tennessee 37831-6460, USA*

[3]*IMPMC, CNRS UMR 7590, Université Pierre et Marie Curie, 75252 Paris, France*

[4]*ISIS Facility, Rutherford Appleton Laboratory, Chilton, Didcot OX11 0QX, United Kingdom*

[5]*Department of Condensed Matter Physics and Materials Science, S. N. Bose National Centre for Basic Sciences, Kolkata 700098, India*

(Received 23 October 2014; revised manuscript received 25 February 2015; published 17 March 2015)

We reinvestigate the pressure dependence of the crystal structure and antiferromagnetic phase transition in $MnTe_2$ using the rigorous and reliable tool of high-pressure neutron powder diffraction. First-principles density functional theory calculations are carried out in order to gain microscopic insight. The measured Néel temperature of $MnTe_2$ is found to show unusually large pressure dependence of 12 K GPa^{-1}. This gives rise to a large violation of Bloch's rule given by $\alpha = \frac{d\log T_N}{d\log V} = -\frac{10}{3} \approx -3.3$, to an α value of -6.0 ± 0.1 for $MnTe_2$. The *ab initio* calculation of the electronic structure and the magnetic exchange interactions in $MnTe_2$ for the measured crystal structures at different pressures indicates the pressure dependence of the Neél temperature α is -5.61, in close agreement with experimental findings. The microscopic origin of this behavior turns out to be dictated by the distance dependence of the cation-anion hopping interaction strength.

DOI: 10.1103/PhysRevB.91.104412 PACS number(s): 75.30.−m, 75.40.Cx

I. INTRODUCTION

In 1966, Bloch [1] studied the pressure variation of the Néel temperature T_N and that of the volume V of several transition-metal (TM) based antiferromagnetic insulators (AFI) and came up with the general relationship

$$\alpha = \frac{d\log T_N}{d\log V} = -\frac{10}{3} \approx -3.3. \quad (1)$$

In the localized-electron limit where perturbative superexchange theory is applicable, the Néel temperature can be related to the effective TM-TM hopping interaction b, charge transfer energy Δ, and Coulomb interaction U as

$$T_N \sim b^2\left[\frac{1}{U} + \frac{1}{2\Delta}\right]. \quad (2)$$

The first term in the above equation is the Anderson superexchange term, and the second term involves the two-electron transfer from the anion. A theoretical rationalization of Bloch's rule comes from the calculations of the variation of the cation-anion transfer integral b^{ca} with the cation-anion bond length r, which varies as r^{-n}. The calculated values [2,3] of n using molecular-orbital theory or the configuration-interaction method on transition-metal oxides and fluorides turn out to be in the range 2.5–3. This leads to $T_N \sim r^{-10} \sim V^{-3.3}$, assuming $b = (b^{ca})^2/\Delta$. Experimentally, Bloch's rule is obeyed by a variety of Mott insulators. However, there are exceptions too. For example, while Bloch's rule is found to be obeyed in $YCrO_3$ and $CaMnO_3$, it was found to fail in $LaMnO_3$ [4]. The failure has been explained in terms of the breakdown of the localized approach used in Bloch's formulation. We note that the cases discussed so far related to the pressure dependence of T_N all involve oxygen or fluorine, i.e., anions with $2p$ electrons. As is well known, the nature of the anionic wave function changes as one moves down the column of the periodic table, from $2p$ to $3p$ series and even more to $4p$ and $5p$ series, affecting the TM-anion bonding. It would therefore be of interest to consider the validity of Bloch's criterion in the case of TM compounds containing anions like Te.

A compound of interest in this context is $MnTe_2$. $MnTe_2$ belongs to a large class of pyrite-type and related marcasite- and arsenopyrite-type compounds MX_2 (M = transition element, X = chalcogen or pnictogen element) with diverse magnetic and electrical properties. They range from insulators to metals or even superconductors. They can be diamagnetic, weakly paramagnetic, ferromagnetic, antiferromagnetic, etc. The magnetic semiconductor $MnTe_2$, which has a pyrite-type crystal structure, as shown in Fig. 1, orders below $T_N \approx 88$ K in a type-I antiferromagnetic structure [5–7] with the propagation vector $\mathbf{k} = (1,0,0)$. The magnetic phase transition at T_N was found to be of second order within experimental resolution [6,7], although the other related manganese dichalcogenides MnS_2 and $MnSe_2$ undergo first-order phase transitions [8–11] at T_N. The magnetic structure of $MnTe_2$ had been the subject of controversy [5,12,13] regarding whether the magnetic structure of $MnTe_2$ is of collinear single-**k** or noncollinear triple-**k** type or whether there is any spin reorientation transition. Burlet *et al.* [7] resolved this controversy and determined the magnetic structure to be of noncollinear triple-**k** type. The structure was found to be stable below T_N down to 4.2 K, the lowest temperature at which the magnetic structure was investigated.

The high-pressure x-ray diffraction was carried out previously [14–18] to study the pressure-induced volume changes in $MnTe_2$, although no detailed structural analysis was carried out in terms of the determination of atomic positions. Also, in a separate study the pressure dependence of the Neél temperature was obtained from resistivity and Mössbauer measurements [19]. The results of these two studies put together show a large violation of Bloch's rule, which, however, has not been stressed before. More importantly, a microscopic understanding of this phenomena has been lacking.

In the present study, we take up this issue by experimentally revisiting the pressure dependence of the structure and magnetic ordering temperature of $MnTe_2$ in terms of

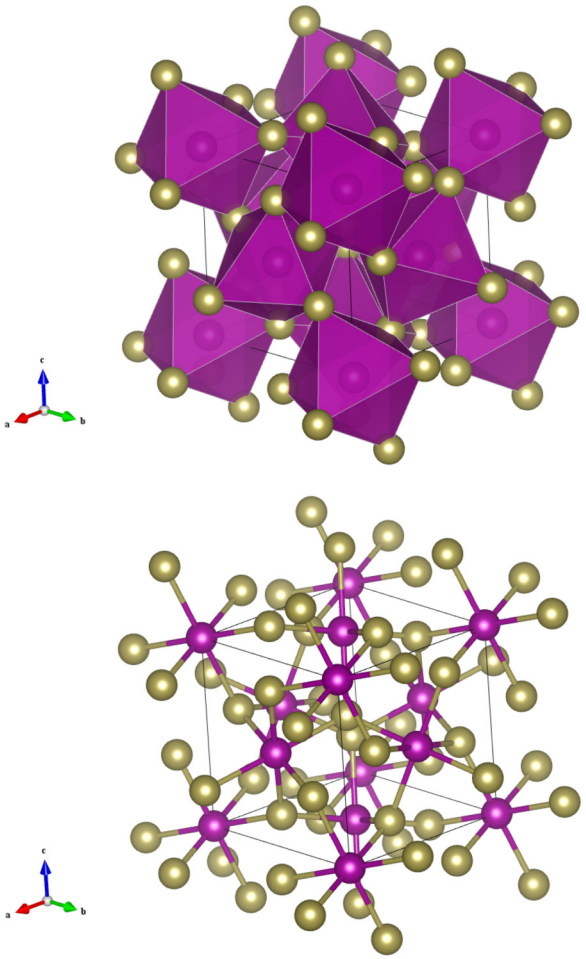

FIG. 1. (Color online) Schematic representation of the crystal structure of $MnTe_2$. Mn atoms are shown as smaller purple spheres, and Te are shown atoms as larger yellow spheres. The top panel shows the polyhedral representation of the $MnTe_6$ octahedra. The bottom panel shows the ball-and-stick version of the same structure in which the distorted octahedral coordination of the Mn by six Te atoms and the distorted tetrahedral coordination of the Te atom by the three Mn and one Te atoms can be seen.

high-pressure powder-neutron-diffraction measurement, together with first-principles density functional theory (DFT) calculation to provide the microscopic understanding. The neutron-diffraction study carried out in the present work is undoubtedly a more reliable tool to measure the magnetic transition temperatures than resistivity or Mössbauer measurements. In addition, the present neutron-diffraction study provides detailed structural information which was not available before, on the basis of which our first-principles calculations have been carried out. Our rigorous study confirms and rationalizes the breakdown of Bloch's rule in $MnTe_2$.

II. METHODOLOGY

High-pressure neutron-diffraction investigations were done on three neutron powder diffractometers, viz., PEARL at the ISIS facility in the United Kingdom; D20 of the Institute Laue-Langevin, Grenoble, France; and SNAP at SNS, Oak Ridge. Pressure was generated by Paris-Edinburgh pressure cells [20,21], and a mixture of 4:1 deuterated methanol:ethanol was used as a pressure-transmitting medium. The PEARL measurements used anvils made of tungsten carbide and a scattering geometry which restricted the available d-spacing range to below 4.2 Å; that is, the magnetic (100) reflection was not recorded. Rietveld refinements of the patterns to the crystal structure were carried out using the GSAS program [22]. The experiments on D20 and SNAP used anvils made of cubic boron nitride [21] and a scattering geometry which gives access to reflections with larger d spacings. The sample temperature was controlled using closed-cycle cryostats; fast cooling to 77 K was achieved by flooding the cell assembly with liquid N_2. The pressure was determined from the known pressure variation [14,15] of the lattice parameter of $MnTe_2$.

DFT calculations on the experimentally measured structures were carried out in the plane-wave basis, within the generalized gradient approximation (GGA) for the exchange-correlation functional, as implemented in the Vienna *Ab initio* Simulation Package [23]. We used Perdew-Burke-Ernzerhof implementation of GGA [24]. The projector augmented-wave potential was used. For the total-energy calculation of different spin configurations, we considered a $2 \times 2 \times 1$ supercell containing a total of 48 atoms in the cell. For the self-consistent field calculation, an energy cutoff of 600 eV and a $4 \times 4 \times 8$ Monkhorst-Pack k-point mesh were found to provide good convergence of the total energy. The missing correlation at the Mn sites beyond GGA was taken into account through supplemented Hubbard U (GGA + U) calculation [25] following the Dudarev implementation, with the choice of $U = 5.0$ eV and Hund's coupling J_H of 0.8 eV. Variation in the U value has been studied and has been found to have no significant effect on the trend.

III. EVOLUTION OF THE STRUCTURAL PARAMETERS UNDER PRESSURE

The pyrite-type crystal structure of $MnTe_2$ in the $Pa\bar{3}$ space group has the Mn atom at $4(a)(000)$ and the Te atom at the $8(c)(xxx)$ position. The cubic lattice parameter a and the Te positional parameter x were refined along with the isotropic atomic displacement parameters of Mn and Te atoms. Figure 2 shows the pressure dependence of the structural parameters of $MnTe_2$, viz., the lattice parameter, the positional parameter x of the Te atom, Mn-Te and Te-Te bond lengths, and the Mn-Te-Mn and Mn-Te-Te bond angles. The results are very remarkable and are contrary to our naive expectation that the Te-Te bond distance would continuously decrease with pressure. Instead, the bond distance seems to increase slightly at lower pressure, but after reaching a maximum at $P = 2$ GPa, it decreases and becomes somewhat flat at about $P = 10$ GPa. The two bond angles also show anomalous pressure dependence. This is expected since all the relevant bond distances and angles are derived from the single Te positional parameter x and the cubic lattice parameter a, which decreases with pressure in the usual way. In contrast, the Mn-Te bond length is highly pressure sensitive and is almost entirely responsible for the pressure-induced volume reduction, suggesting relatively weak Mn -Te bonds which are susceptible to changes upon application of pressure. The remarkable pressure response of the Te-Te bond distance and

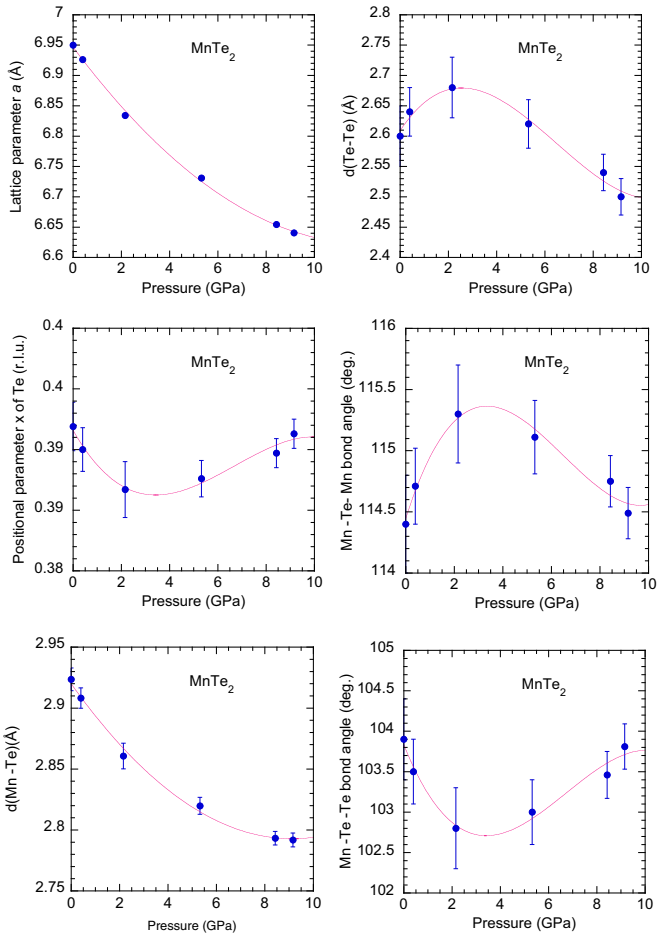

FIG. 2. (Color online) Pressure dependence of the structural parameters of $MnTe_2$ determined from the data measured on the PEARL diffractometer at the ISIS facility. The red solid lines are guides to the eye.

Mn-Te-Mn and Mn-Te-Te angles should be reflected in the pressure dependence of the superexchange interaction that decides the pressure variation of the Néel temperature, as obtained in our first-principles calculations. Figure 3 shows the pressure variation of the unit cell volume of $MnTe_2$ and its fit with Murnaghan equation of state. The fit gave $B_0 = 34.6 \pm 1.0$ GPa and $B_0' = 8.8 \pm 0.4$, where B_0 is the bulk modulus and B_0' is its pressure derivative. The values agree well with the values determined previously from high pressure x-ray diffraction [14,15].

IV. MEASURED PRESSURE VARIATION OF T_N

The antiferromagnetic phase transition of $MnTe_2$ was first investigated at ambient pressure with the sample (outside the pressure cell) fixed to the cold tip of a standard orange cryostat. Figure 4 shows neutron-powder-diffraction intensities of the 100 and 110 magnetic peaks along with the 111 nuclear peak at several temperatures below and close to the antiferromagnetic Néel temperature $T_N = 88$ K. Figure 5(a) shows the temperature variation of the integrated intensity of the 100 magnetic Bragg peak. The intensity of this reflection decreases continuously with increasing temperature and becomes zero at

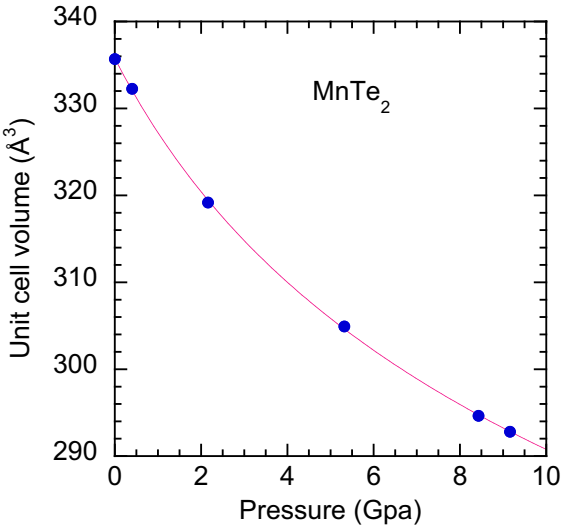

FIG. 3. (Color online) Pressure variation of the unit cell volume of $MnTe_2$ and its fit to the Murnaghan equation of state that gives $B_0 = 34.6 \pm 1.0$ GPa and $B_0' = 8.8 \pm 0.4$.

about $T_N \approx 88$ K. The data just below T_N could be fitted by a power-law exponent

$$I = I_0 \left(\frac{T_N - T}{T_N} \right)^{2\beta}, \tag{3}$$

where I is the integrated intensity, I_0 is the saturation value of the intensity at $T = 0$, T_N is the critical temperature, and β is the power-law exponent. The least-squares fit of the data in the temperature range from $T = 60$ to $T = 88$ K gave $\beta = 0.29 \pm 0.04$ and a Néel temperature $T_N = 88 \pm 2$ K. The fitted value of the Néel temperature was used to determine the reduced temperature $t = (T_N - T)/T_N$. We then produced the standard log-log plot shown in Fig. 5(b) to extract the critical exponent $\beta = 0.29$ from the slope that agreed well with that determined by the least-squares fit.

Figure 6 shows neutron-powder-diffraction intensities of the 100 and 110 magnetic peaks along with the 111 nuclear peak of $MnTe_2$ under $P = 4.75$ GPa at several temperatures below and above the antiferromagnetic Néel temperature. It is immediately noticed that the application of hydrostatic pressure $P = 4.75$ GPa increases the Néel temperature $T_N = 88$ K of $MnTe_2$ substantially. By fitting the temperature dependence of the intensity of the 100 magnetic peak and fitting the data by a power law we determine $T_N = 145 \pm 7$ K. Figure 7(a) shows this fit. Similarly, we determined the Néel temperatures of $MnTe_2$ at several pressures. The result is shown in Fig. 7(b). The obtained trend agrees well with that obtained from resistivity and Mössbauer spectroscopy [19], as also shown in Fig. 7(b). The neutron-diffraction results show that T_N of $MnTe_2$ increases linearly in the pressure range 0–8 GPa at a rate of about 12 K GPa^{-1}, determined from the slope of the linear plot. From this linear relationship we calculated the T_N values for the pressures at which we determined the lattice and positional parameters of $MnTe_2$ from the high-pressure neutron-diffraction experiment on the PEARL diffractometer. Figure 7(c) shows the log-log plot of Néel temperature T_N vs the unit-cell volume of $MnTe_2$.

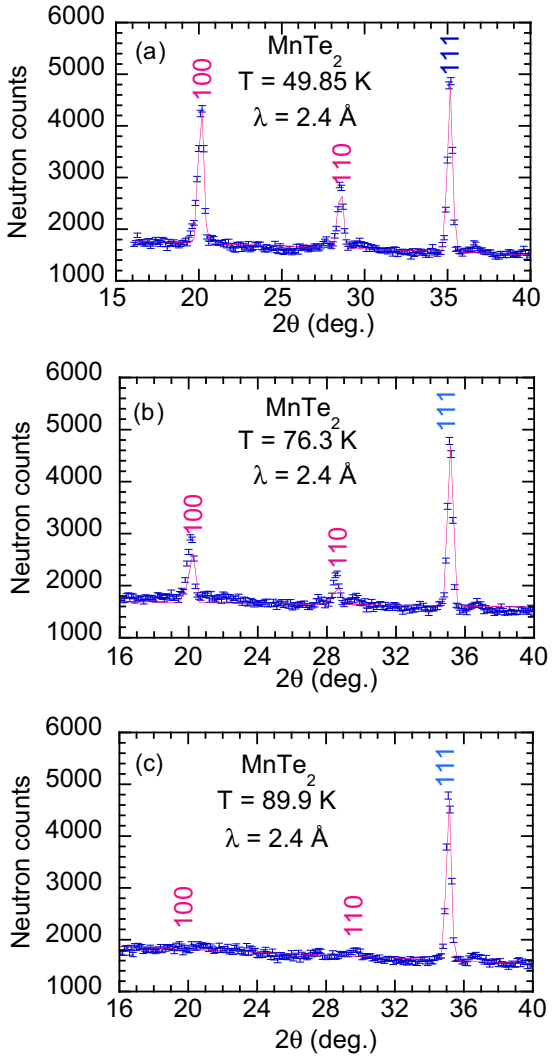

FIG. 4. (Color online) Neutron-powder-diffraction intensities of the 100 and 110 magnetic peaks along with the 111 nuclear peak at several temperatures below and close to the antiferromagnetic Néel temperature $T_N = 88$ K. The data have been measured on the D20 diffractometer of the Institut Laue-Langevin in ambient pressure. The red lines are the results of Gaussian fits of the Bragg peaks.

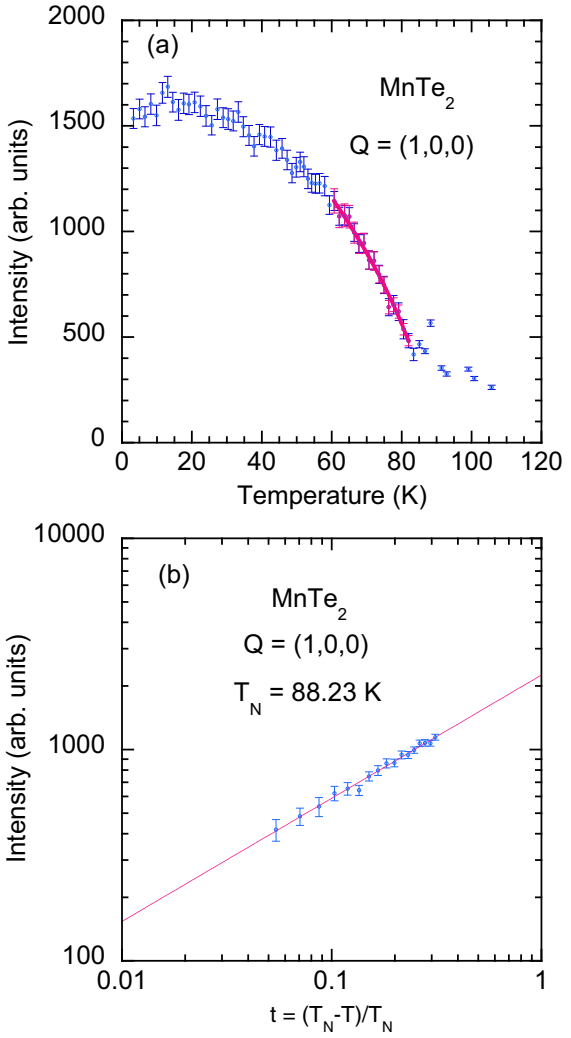

FIG. 5. (Color online) (a) Temperature variation of the integrated intensity of the 100 magnetic Bragg peak. The red line is the result of the least-squares fit of the data. The temperature range of the data used for the fit is also given by the temperature range of the red line. The least-squares fit gives the power-law exponent $\beta = 0.29 \pm 0.04$ and a Néel temperature $T_N = 88 \pm 2$ K. (b) Log-log plot of the intensity of the 100 magnetic reflection vs the reduced temperature.

The slope of this plot gives $\alpha = -6.0 \pm 0.1$, which is much larger than the Bloch rule value of $\alpha = -3.3$. Our result therefore points towards a spectacular breakdown of Bloch's rule in $MnTe_2$. We note that transition to a nonmagnetic state of the Mn^{2+} ions in $MnTe_2$ was reported [19] from the resistivity and Mössbauer study and was also evidenced by the pressure variation of infrared reflectivity investigated by Mita *et al.* [26]. Our experiments, however, did not show the volume collapse observed in high-pressure x-ray diffraction experiments [14,15]. It is therefore plausible that we did not reach the transition pressure during the present high-pressure neutron-diffraction experiments. The exact pressure at which the transition to a nonmagnetic state is expected to happen depends sensitively on the experimental conditions.

The present neutron-diffraction data contain, in principle, the magnetic moment information because neutron diffraction probes both crystal and magnetic structures, and the intensities of the magnetic reflections when put to the absolute scale by using the intensities of the nuclear reflections can give the ordered moment values. However, this is not an easy task, especially in a high-pressure experiment using a large Paris-Edinburg pressure cell. The high absorption of the pressure cell and also a very high background hinder accurate determination of the nuclear and magnetic intensities. In the present case, despite our efforts, the determination of the pressure dependence of the ordered moment from the neutron-diffraction data was not successful. We know, however, from our calculations (using the pressure dependence of the structural parameters) that the ordered moment of Mn ions does not change at all (or very little) in the investigated range of 0–9 GPa. The present high-pressure neutron-diffraction data seem to support this result. The intensity ratio of the magnetic and nuclear Bragg peaks does not change very much and is within the accuracy in the pressure range investigated.

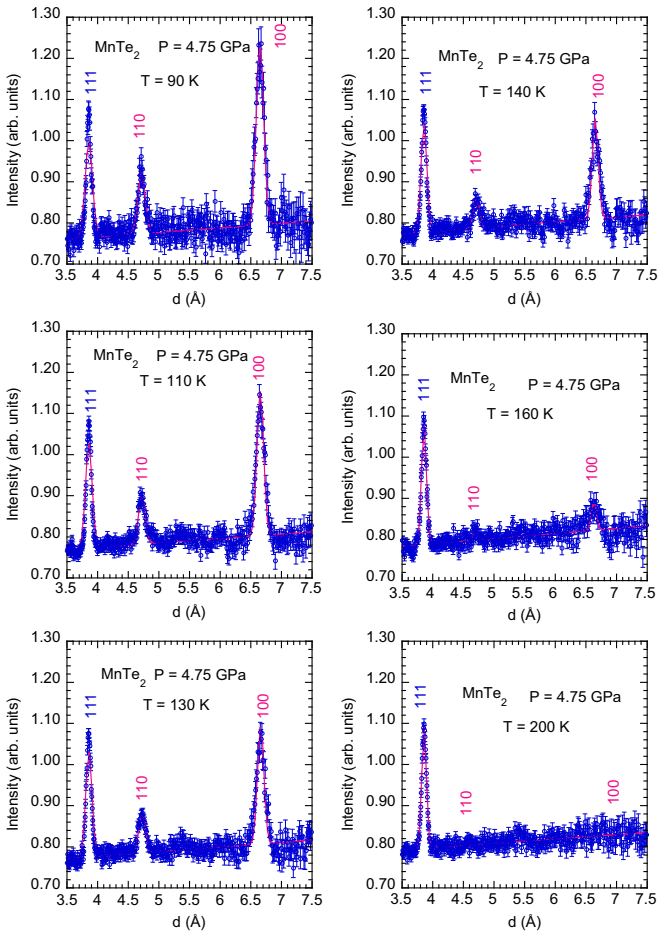

FIG. 6. (Color online) Neutron-powder-diffraction intensities of the 100 and 110 magnetic peaks along with the 111 nuclear peak of $MnTe_2$ under $P = 4.75$ GPa at several temperatures below and above the antiferromagnetic Néel temperature measured on the SNAP diffractometer of the SNS of Oak Ridge National Laboratory. The red lines are results of Gaussian fits of the Bragg peaks.

V. FIRST-PRINCIPLES STUDY

A. Calculated pressure variation of Neél temperature

To gain understanding of the significantly large pressure dependence of the Neél temperature in $MnTe_2$ we carried out a theoretical investigation in terms of first-principles DFT calculations. Figure 8 shows the comparison of the spin-polarized density of states of $MnTe_2$ at ambient pressure and at a pressure of 9.16 GPa, the highest pressure studied in the present calculations. The spin-polarized calculations within GGA + U gave rise to a magnetic moment of $4.6\mu_B$ ($4.5\mu_B$) at Mn site together with a moment of $0.03\mu_B$ ($0.05\mu_B$) at the Te site for the ambient ($P = 9.16$ GPa) pressure condition, suggesting the high-spin state of Mn at both ambient and high-pressure conditions, in agreement with experimental findings. Both ambient-pressure and high-pressure phases were found to be insulating, with a gap at the Fermi energy, marked as zero in Fig. 8. The Mn d states are fully occupied in the majority-spin channel and completely empty in the minority-spin channel, in agreement with the high-spin state of Mn in its nominal 2+ valence state. The comparison of the density of states between ambient pressure and high pressure, however, shows

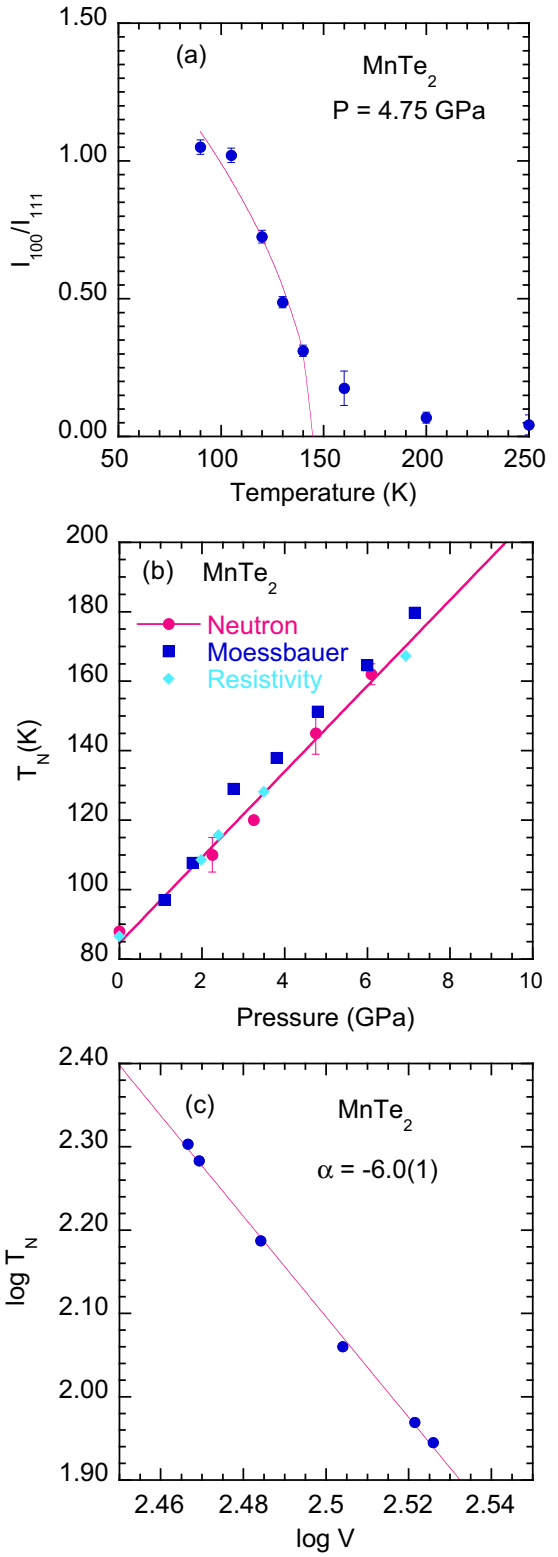

FIG. 7. (Color online) (a) Temperature variation of the intensity of the 100 reflection of $MnTe_2$ at $P = 4.75$ GPa and its power-law fit. The red line is the result of the least-squares fit of the data. The power-law fit yields $T_N = 145 \pm 7$ K. (b) Pressure variation of the Néel temperature of $MnTe_2$. The Mössbauer and the resistivity data are taken from Vulliet *et al.* [19]. The linear fit of the neutron data yields $\frac{dT_N}{dP} = 12$ K GPa^{-1}. (c) Log-log plot of the Néel temperature T_N vs the unit-cell volume of $MnTe_2$. The red straight line is the result of the linear fit of the data, yielding $\alpha = -6.0 \pm 0.1$.

enhancement of the Mn d-band width by $\approx$1 eV, indicating the hopping interaction between Mn d and Te p increases substantially in moving from the ambient- to high-pressure phase.

To extract the various magnetic interactions J between the Mn spins, we calculated the GGA + U total energies for various configurations of Mn spins and mapped the total energy onto an underlying $S = 5/2$ Heisenberg model. Calculations were carried out for six different pressures: 0.0, 0.4, 2.16, 5.32, 8.43 and 9.16 GPa. The dominant magnetic interactions considered in our calculation of J were J_1, between the first-nearest-neighbor (1NN) Mn atoms, connected to each other by the corner-shared Te atoms, and J_2, between the second-nearest-neighbor (2NN) Mn atoms, connected to each other through Te-Mn-Te bridges.

Apart from the ferromagnetic (FM) configuration, with all Mn spins in the supercell pointing in the same direction, two different antiferromagnetic (AFM) configurations, AFM1 and AMF2, were considered, with antiferromagnetic arrangement of 1NN Mn and 2NN Mn spins. The GGA + U total energies corresponding to AFM configurations, measured with respect to the energy of the FM configuration, turned out to be negative for all the studied pressures, in accordance with the dominance of antiferromagnetic interactions. Extracting J_1 and J_2 by mapping the total energy onto the spin Hamiltonian, given by $H = -J_1 \sum_{nn} S^i_{\rm Mn} S^j_{\rm Mn} - J_2 \sum_{2nn} S^i_{\rm Mn} S^j_{\rm Mn}$, gave J_2 as a small fraction of J_1, with $J_1/J_2 = 0.09$ at ambient pressure and 0.12 at 9.16 GPa, suggesting the magnetism is primarily governed by J_1. The pressure dependence of exchange interactions is shown in Fig. 9.

With the knowledge of J, we calculated the Neél temperature T_N using mean-field theory, given by $T_N^{mf} = \frac{S(S+1)J_0}{3K_B}$, where J_0 is the net effective interaction $12J_1 + 4J_2$, $S = 5/2$, and K_B is the Boltzmann constant. Mean-field theory is expected to overestimate the transition temperature, although the trend is expected to be captured well, which is governed by J. The computed $\log[T_N(P)/T_N(0)]$ plotted as a function of $\log(V)$ is shown in Fig. 10. The straight-line fit to the calculated data points gives rise to a slope of -5.61, which is close to the experimental estimate of -6.0 ± 0.1. Both our experimental results and *ab initio* calculations thus establish that Bloch's rule is largely violated in $MnTe_2$. In the following we theoretically investigate the microscopic origin of this behavior.

B. Microscopic origin of the breakdown of Bloch's rule

Bloch's rule has been found to be very successful for many magnetic insulators, especially the transition-metal oxides and fluorides. The following question then arises: what makes the Bloch's rule fail for $MnTe_2$? In order to explore this, we extracted the hopping interactions b^{ca}, where c and a signify Mn and Te, respectively, by carrying out Nth-order muffin-tin-orbital (NMTO) based NMTO-downfolding calculations [27]. This involved the construction of the real-space representation of the Mn d-O p Hamiltonian in the Wannier function basis out of the full DFT calculations by integrating out all the degrees of freedom other than Mn d and Te p. Our NMTO-downfolding calculations to extract the dependence of b^{ca} on the cation-anion distance r gave $b^{ca} \sim \frac{1}{r^{4.2}}$, instead of $b^{ca} \sim \frac{1}{r^{2.5}}$ assumed for the derivation of Bloch's rule. This gives $T_N \sim \frac{1}{r^{17}} \sim \frac{1}{V^{5.67}}$, which is very close to the estimate obtained from total-energy calculations, as well as from the experiment. This points to the fact that violation of Bloch's rule in the case of $MnTe_2$ is caused by the deviation in the distance dependence of b^{ca} from the $\frac{1}{r^{2.5}}$ behavior, rather than that by U or Δ. We find that the distance dependence of b^{ca} found for $MnTe_2$ is more like the canonical behavior [28], in which the interatomic matrix elements are supposed to scale with distance as $\frac{1}{r^{l+l'+1}}$, where l and l' are the angular momenta of the orbitals involved. In the case of several TM oxides, on the other hand, analysis of DFT band structure [29] gave rise to a $\frac{1}{r^{l+l'}}$ behavior, similar to that obtained from molecular-orbital theory or the configuration-interaction method for $KNiF_4$, MnO, or MnF_2 [2,3]. This presumably

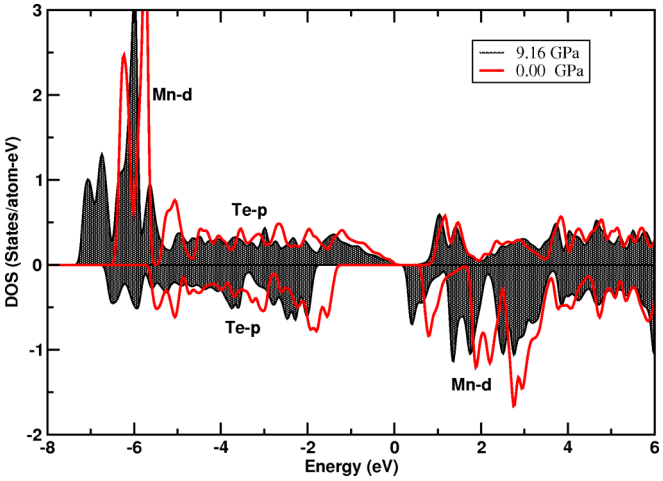

FIG. 8. (Color online) Comparison of the GGA + U density of states between the ambient-pressure (solid line) and high-pressure (shaded area) phases. The energies are measured with respect to GGA + U Fermi energy. The states of dominant Mn d and Te p characters have been marked.

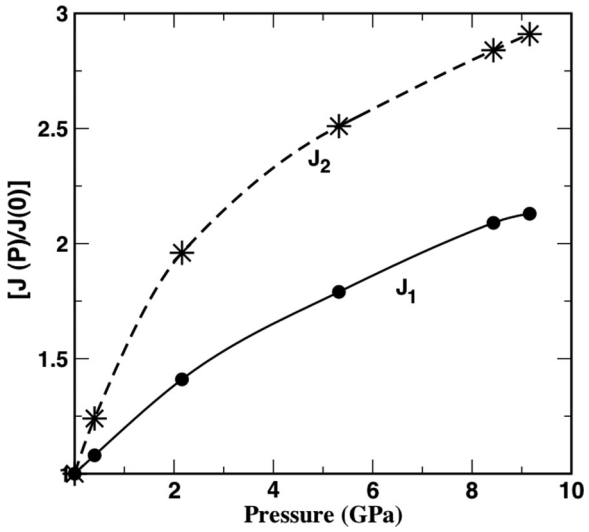

FIG. 9. The ratio of J at pressure P and that at ambient pressure (denoted as $P = 0$), plotted as a function of pressure. The solid line corresponds to J_1, and the dashed line corresponds to J_2.

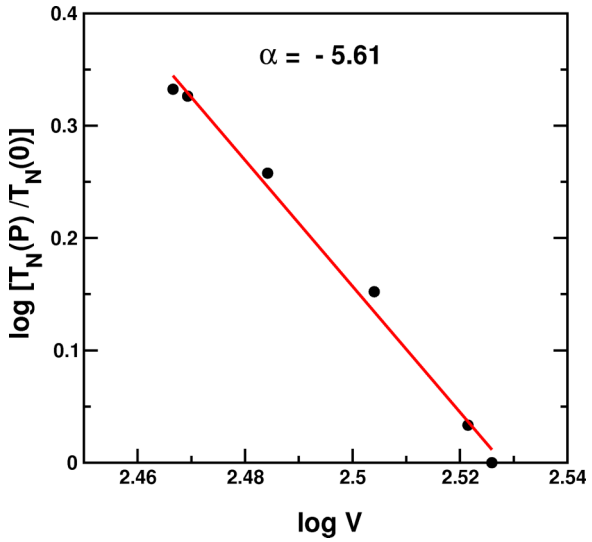

FIG. 10. (Color online) Log-log plot of $T_N(P)/T_N(0)$ vs volume. The linear fit to the data points is shown by the line, which has a slope of $\alpha = -5.61$.

originates from the differential nature of Te $4p$ wave functions compared with those of $2p$ or $3p$, which together with the nonmonotonic pressure dependence of the position parameter x influences the superexchange interaction in a differential manner.

VI. SUMMARY

In conclusion, the Néel temperature of $MnTe_2$ was found to show an unusually large pressure dependence of about 12 K GPa^{-1}, which has been confirmed in the present study through more rigorous and reliable high-pressure neutron-diffraction experiments compared with that in the literature, as well as through first-principles density functional theory calculations. Our measured pressure dependence of the Néel temperature and unit-cell volume gave $\alpha = -6.0 \pm 0.1$, which is much larger than that expected from Bloch's rule, $\alpha = \frac{d \log T_N}{d \log V} = -\frac{10}{3} \approx -3.3$. The calculated pressure dependence of the Néel temperature gave rise to $\alpha = -5.61$, in good agreement with the experimental estimate. We provided a microscopic understanding of this behavior in terms of the distance dependence of the Mn-Te hopping interaction upon application of pressure, which showed significant deviation from that of NiF_4, MnO, or MnF_2 [2,3].

Finally, the large pressure dependence of magnetic interactions and magnetic ordering temperature provide us with a way to tune the properties of magnetic materials, which could lead to important technological applications. The present study should have important bearing on this topic.

ACKNOWLEDGMENT

Research conducted at ORNL's Spallation Neutron Source, was sponsored by the Scientific User Facilities Division, Office of Basic Energy Sciences, US Department of Energy.

[1] D. Bloch, J. Phys. Chem. Solids **27**, 881 (1966).
[2] D. W. Smith, J. Chem. Phys. **50**, 2784 (1969).
[3] K. N. Shrivastava and V. Jaccarino, Phys. Rev. B **13**, 299 (1976).
[4] J.-S. Zhou and J. B. Goodenough, Phys. Rev. Lett. **89**, 087201 (2002).
[5] J. M. Hastings, N. Elliott, and L. M. Corliss, Phys. Rev. **115**, 13 (1959).
[6] T. Chattopadhyay and H. Fjellvag, Phys. Lett. A **120**, 44 (1987).
[7] P. Burlet, E. Ressouche, B. Malaman, R. Welter, J. P. Sanchez, and P. Vulliet, Phys. Rev. B **56**, 14013 (1997).
[8] J. M. Hastings and L.-M. Corliss, Phys. Rev. B **14**, 1995 (1976).
[9] T. Chattopadhyay, H. G. von Schnering, and H. A. Graf, Solid State Commun. **50**, 865 (1984).
[10] T. Chattopadhyay, T. Brückel, and P. Burlet, Phys. Rev. B **44**, 7394 (1991).
[11] T. Chattopadhyay, J. Rossat-Mignod, and H. Fjellvåg, Solid State Commun. **63**, 65 (1987).
[12] M. Pasternak and A. M. Spijkervet, Phys. Rev. **181**, 574 (1969).
[13] J. M. Hastings, L. M. Corliss, M. Blume, and M. Pasternak, Phys. Rev. B **1**, 3209 (1970).
[14] H. Fjellvåg, A. Kjekshus, T. Chattopadhyay, H. D. Hochheimer, W. Hönle, and H. G. von Schnering, Phys. Lett. A **112**, 411 (1985).
[15] H. Fjellvåg, W. A. Grosshans, W. Hönle, and A. Kjekshus, J. Magn. Magn. Mater. **145**, 118 (1995).
[16] T. Chattopadhyay and H. G. von Schnering, J. Phys. Chem. Solids **46**, 113 (1985).
[17] T. Chattopadhyay, H. G. von Schnering, and W. A. Grosshans, Phys. B (Amsterdam, Neth.) **139–140**, 305 (1986).
[18] S. A. J. Kimber, A. Salamat, S. R. Evans, H. O. Jeschke, K. Muthukumar, M. Tomić, F. Salvat-Pujol, R. Valenti, M. V. Kaisheva, I. Zizak, and T. Chatterji, Proc. Natl. Acad. Sci. USA **111**, 5106 (2014).
[19] P. Vulliet, J. P. Sanchez, D. Braithwaite, M. Amanowicz, and B. Malaman, Phys. Rev. B **63**, 184403 (2001).
[20] J. M. Besson, R. J. Nelmes, G. Hamel, J. S. Loveday, G. Weill, and S. Hull, Phys. B (Amsterdam, Neth.) **180–181**, 907 (1992).
[21] S. Klotz, Th. Strässle, G. Rousse, G. Hamel, and V. Pomjakushin, Appl. Phys. Lett. **86**, 031917 (2005).
[22] R. B. von Dreele and A. C. Larson, Los Alamos National Laboratory, Report No. LAUR 86-746, 1986 (unpublished).
[23] G. Kresse and J. Hafner, Phys. Rev. B **47**, 558(R) (1993); G. Kresse and J. Furthmüller, *ibid.* **54**, 11169 (1996).
[24] J. P. Perdew, K. Burke, and M. Ernzerhof, Phys. Rev. Lett. **77**, 3865 (1996).
[25] S. L. Dudarev, G. A. Botton, S. Y. Savrasov, C. J. Humphreys, and A. P. Sutton, Phys. Rev. B **57**, 1505 (1998).
[26] Y. Mita, Y. Ishida, M. Kobayashi, and S. Endo, Acta Phys. Pol. A **113**, 617 (2008).
[27] O. K. Andersen and T. Saha-Dasgupta, Phys. Rev. B **62**, R16219 (2000).
[28] O. K. Andersen, W. Klose, and H. Nohl, Phys. Rev. B **17**, 1209 (1978).
[29] P. Mahadevan, N. Shanthi, and D. D. Sarma, Phys. Rev. B **54**, 11199 (1996).